# MAPPING TIDAL AND SEASONAL MOVEMENTS OF THE MAXIMUM TURBIDITY ZONE IN ESTUARINE WATERS FROM REMOTELY SENSED (SPOT, LANDSAT) DATA. A SEMI-EMPIRICAL APPROACH.

*David Doxaran[1], Samantha J. Lavender[1] and Jean-Marie Froidefond[2]*

1. University of Plymouth, Institute of Marine Studies, PL4 8AA, Plymouth, UK; {david.doxaran/s.lavender}(at)plymouth.ac.uk
2. University of Bordeaux 1, DGO, 33405 Talence, France; jm.froidefond(at)epoc.u-bordeaux1.fr

## ABSTRACT

The study concerns the quantification of suspended sediments in turbid estuarine waters from high spatial resolution remotely sensed data (SPOT-HRV, Landsat-ETM+). It is applied to the following areas: the Gironde and the Loire estuaries (France), where suspended sediment concentrations (*SPM*) in surface waters vary from 10 to 2000 mg $l^{-1}$.

The methodology is essentially empirical. Based on in situ optical measurements, calibration relationships are established between the remote sensing reflectance ($R_{rs}$) signal and *SPM*. These relationships, obtained using reflectance ratios between near-infrared (NIR) and visible (VIS) wavebands, are relatively independent of the sediment grain-size and mineralogy, and of the illumination conditions (e.g. the cloud cover). Consequently, they can be applied to satellite images, even if no simultaneous in situ measurements were carried out concurrently with the satellite overpass.

A bio-optical model is used to explain the obtained empirical results. It relates the inherent and apparent optical properties of the considered estuarine waters. Scattering by sediments is modelled using the Mie theory. Absorption by sediments is modelled according to the existing knowledge in the domain. The modelled optical properties are validated by comparison with in situ measurements.

The established calibration relationships allow an accurate estimation of concentrations, once satellite data are corrected for atmospheric effects. Resulting *SPM* maps permit to observe the seasonal movements of the maximum turbidity zone (MTZ) and the resuspension phenomena in the Gironde estuary.

**Keywords:** Estuary, sediment, satellite, turbid waters

## INTRODUCTION

In coastal waters, estuaries are complex environments where dissolved and particulate matter drained by rivers in upland basins are mixed with marine substances. As a consequence of the tidal asymmetry and the residual density circulation, a MTZ is formed where most of the suspended particles are trapped. Depending on the upland basins, these particles are mainly cohesive sediments (clays and silts), which settle and can form fluid mud layers during neap tides. The presence of a MTZ strongly affects biological processes. The main influence of turbidity is the limitation of light penetration in the water column, which is a factor controlling primary production. The understanding of fine sediment transport, notably in the high-turbidity zone, is also necessary to predict the fate of eventual pollutants and to design dredging strategies.

Spatial remote sensing is the most efficient tool for mapping the suspended particle concentrations and observing seasonal movements of turbidity in estuaries. This information is essential in the initialisation and validation of numerical hydro-sedimentary models (1,2), in order to quantify sedimentary fluxes and estimate the fluvial solid discharges to the ocean. However, the signal meas-

ured by ocean colour satellite sensors is complicated in coastal waters because of the presence of terrestrial substances, such as coloured dissolved organic matter (CDOM) and suspended sediments in addition to phytoplankton. In estuaries, the characteristics (grain size, mineralogy) of the suspended particles vary depending on the upland basins, river discharge, tidal cycles and flocculation processes. These variations affect their optical properties. As a consequence, it is difficult to establish invariant and improved algorithms to quantify SPM (3,4,5,6). Calibration of remote sensing data usually requires simultaneous in situ measurements during satellite data acquisition, which involves systematic costly field experiments. Recent works in highly turbid estuarine waters have shown that simple and refined SPM quantification algorithms can be established using reflectance ratios between NIR and VIS bands. The established calibration curves between reflectance ratios and SPM are relatively insensitive to the sediment characteristics, and also relatively insensitive to the illumination conditions (e.g. cloud cover) concurrent with the field measurements (7,8,9).

The first objective of this study is to present a simple method that can be used to quantify suspended sediments in turbid coastal waters from satellite data, without taking simultaneous field measurements. The validity and limits of calibration relationships established in two West European estuaries are discussed. The second objective is to apply the method to satellite data, previously corrected for the atmospheric effects, in order to observe the tidal and seasonal movements of the MTZ in a macrotidal estuary, the horizontal sediment transport and resuspension phenomena. The two selected estuaries are the Gironde and the Loire, in France; the selected satellite sensors are SPOT-HRV and Landsat-ETM+.

## METHODS

### Theory:

The radiometric measurement recorded at the top of the atmosphere by passive satellite sensors is the upwelling radiance $L^*$. Neglecting unisotropy, these measurements can be converted into the commonly used top of atmosphere reflectance $R^*$ (10):

$$R^* = \frac{\pi L^*}{\cos(\theta_s)\, E_s} \tag{1}$$

where $\theta_s$ is the solar zenith angle, $E_s$ is the solar irradiance at the top of the atmosphere. The optical parameters presented in this paragraph depend on the wavelength ($\lambda$), but the subscript $\lambda$ is omitted for clarity.

In the single scattering assumption, reflectance at the top of the atmosphere can be written as the sum of atmospheric and water contributions (6,11):

$$R^* = R_{aer} + R_{ray} + R_g + t\,R_w \tag{2}$$

where $R_{aer}$ is the reflectance due to aerosols, $R_{ray}$ is the Rayleigh reflectance due to scattering by air molecules, $R_g$ is the reflectance from the solar beam, $t$ is the diffuse atmospheric transmittance and $R_w$ is the water reflectance. If data are screened for sunglint, the term $R_g$ can be ignored (6).

The purpose of the satellite atmospheric correction is the determination of the atmospheric terms in eq. (2), their subtraction from the top of atmosphere reflectance and retrieval of the water reflectance $R_w$.

For oceanographic remote sensing applications, a specific water reflectance signal called remote sensing reflectance $R_{rs}$ has been defined (12):

$$R_{rs} = \frac{L_w}{E_d} \tag{3}$$

where $L_w$ is the water-leaving radiance and $E_d$ is the downwelling irradiance incident on the water surface. The signal $R_w$ retrieved from satellite data is the ratio between the above water upwelling radiance multiplied by $\pi$ and the downwelling irradiance just above the water surface (see, for example, (10)). It is equivalent to $R_{rs}$ multiplied by $\pi$ (12).

$R_{rs}$ can be related to the inherent optical properties of the water body (13,14), namely the absorption and backscattering coefficients *a* and $b_b$, by taking into account some geometrical parameters resulting from the air - water surface transfer, and the bidirectional aspects (15,16). In the case of the turbid waters of the Gironde estuary, this relationship can be approximately written as (8):

$$R_{rs} \approx 0.524 \frac{f}{Q} \frac{b_b}{a + b_b} \tag{4}$$

where *f* is a dimensionless function depending on illumination conditions and water types (15, 16); the mean value of *f* is 0.324 for a Sun close to the zenith (16). *Q* is defined as the ratio between the upwelling radiance $L_u$ and the upwelling irradiance signals, at null depth (i.e. just below the surface). It would be $\pi$ if the $L_u$ distribution was isotropic, but may vary between approximately 3.1 and 5.6 sr (16,17).

In turbid sediment-dominated waters, the contribution of phytoplankton can be neglected in a first approximation, and the total coefficients *a* and $b_b$ can be written as the sum of the contributions of pure water (*w*), dissolved organic matter (*y*) and sediments (*s*) (18):

$$a = a_w + a_y + a_s \tag{5}$$

$$b_b = b_{bw} + b_{bs} \tag{6}$$

Both the absorption and backscattering coefficients of sediments $a_s$ and $b_{bs}$ can be modelled as functions proportional to the sediment concentration. As a consequence, the $R_{rs}$ signal can be directly related to SPM, according to an empirical or semi-empirical formula (e.g. 7).

**Material and methods**

In order to retrieve horizontal distributions of SPM in estuaries, the following procedure was applied. Numerous shipboard $R_{rs}$ measurements were recorded in different estuarine locations, and associated with water samples taken within surface waters. The collected data were used to find out an invariant empirical relationship between $R_{rs}$ in SPOT-HRV and Landsat-ETM+ bands with SPM. Satellite data from the Gironde and Loire estuaries were corrected for atmospheric effects, then converted into SPM using the established empirical relationships. The satellite images were selected at different periods of the year, in order to observe the seasonal movements of the MTZ. Regular vertical turbidity profiles were recorded in different stations within the estuaries, to explain and interpret the SPM maps produced from the satellite data.

Satellite atmospheric correction was computed using the 6S radiative transfer code (10). The 6S code solves the radiative transfer equation considering separately absorption and scattering effects. Eq. (2) is thus rewritten:

$$R^* = t_g \left( \rho_{aer} + \rho_{ray} + t_{ray} t_{aer} R_w \right) \tag{7}$$

where $t_g$ is the total gaseous transmittance, $\rho_{ray}$ and $\rho_{aer}$ are the Rayleigh and aerosol reflectances ignoring absorption effects, and $t_{ray}$ and $t_{aer}$ are the Rayleigh and aerosol transmittances.

The atmospheric gaseous composition was estimated by selecting appropriate predefined models in 6S (Midlatitude Summer, Midlatitude Winter), which estimate the gaseous components in eq. (7), namely $t_g$, $\rho_{ray}$ and $t_{ray}$, for satellite bands.

The aerosol components cannot be predicted *a priori*. *In situ* wind direction and visibility data can provide information on aerosols (7), but the common method used to estimate composition and concentration of aerosols is the black target one (19). This method is based on the assumption that the incident solar light in NIR bands is totally absorbed by clear waters (i.e. water with very low suspended particle concentrations). As a consequence, the water-leaving radiance over such clear waters is zero in the NIR and the measured signal onboard the satellite is only due to the atmosphere (i.e. $R_w$ = 0). The aerosol contribution in the NIR is then estimated according to:

$$R^* - t_g \rho_{ray} = t_g \rho_{aer} = R_{aer} \tag{8}$$

Considering two bands in the NIR, $\lambda_{NIR1}$ and $\lambda_{NIR2}$, the Ångström coefficient *n*, defined as (20):

$$n = -\ln\left[\frac{R_{aer}(\lambda_{NIR1})}{R_{aer}(\lambda_{NIR2})}\right] \Big/ \ln\left[\frac{\lambda_{NIR1}}{\lambda_{NIR2}}\right] \tag{9}$$

can be used to determine the aerosol contribution in the remaining visible bands ( $\lambda_{VIS}$ ) (10):

$$R_{aer}(\lambda_{VIS}) = \mathrm{R}_{\mathrm{aer}}(\lambda_{NIR2})\left(\frac{\lambda_{VIS}}{\lambda_{NIR2}}\right)^{-n} \tag{10}$$

$t_{aer}$ is the remaining parameter to be determined. The 6S aerosol model, initially selected according to the available meteorological data (notably wind speed and direction), is fitted in order to retrieve the calculated $R_{aer}$ and gives the needed $t_{aer}$ values. Eq. (7) can then be solved and the water reflectance signal retrieved.

For calibration of satellite data, field optical measurements were carried out using a Spectron SE-590 spectroradiometer. This sensor records a radiance signal between 380 and 1100 nm in 256 channels, with an acceptance angle of 6° (field of view). The measurement procedure and determination of the $R_{rs}$ signal have been previously described (7,8,9). To summarise, three successive above-water radiance measurements were recorded: the upwelling radiance $L_u$, sensor pointing towards nadir; the downwelling radiance $L_d$, sensor pointing towards a Spectralon target; the sky radiance $L_s$, sensor pointing towards the zenith.

The measured $L_u$ signal was corrected for the skylight reflection effects on the water surface by subtracting a certain percentage $\rho$ of the $L_s$ signal (12,21):

$$L_w = L_u - \rho L_s \tag{11}$$

Depending on the cloud cover, the $\rho$ values were taken according to the results obtained by Mobley (12).

As the Spectralon plate is a Lambertian target, the downwelling irradiance $E_d$ was:

$$E_d = \pi L_d / R_p \tag{12}$$

where $R_p$ is the reflectance factor of the Spectralon plate.

The $R_{rs}$ signal was finally given by:

$$R_{rs} = R_p \frac{L_u - \rho L_s}{\pi L_d} \quad (13)$$

Then, from the recorded hyperspectral values, $R_{rs}$ in wavebands of the selected satellite sensors was determined by taking into account their spectral sensitivity. For each optical measurement, a water sample was collected at 0.5 metre below the surface, then filtered (filters Whatman GF/F) in order to determine the SPM concentration.

**Data**

A total of 132 field measurements were carried out in the Gironde estuary (Figure 1) between 1996 and 2001, in order to calibrate satellite data; the SPM range is: 10 – 2000 mg $l^{-1}$ (9). A total of 66 similar field measurements were carried out in the Loire estuary in 2002; the SPM range is: 40 – 2600 mg $l^{-1}$ (9). These datasets are representative of different tidal and seasonal conditions in the two estuaries. Each one of the measurements represents a calibration point between the $R_{rs}$ signal in satellite bands and SPM.

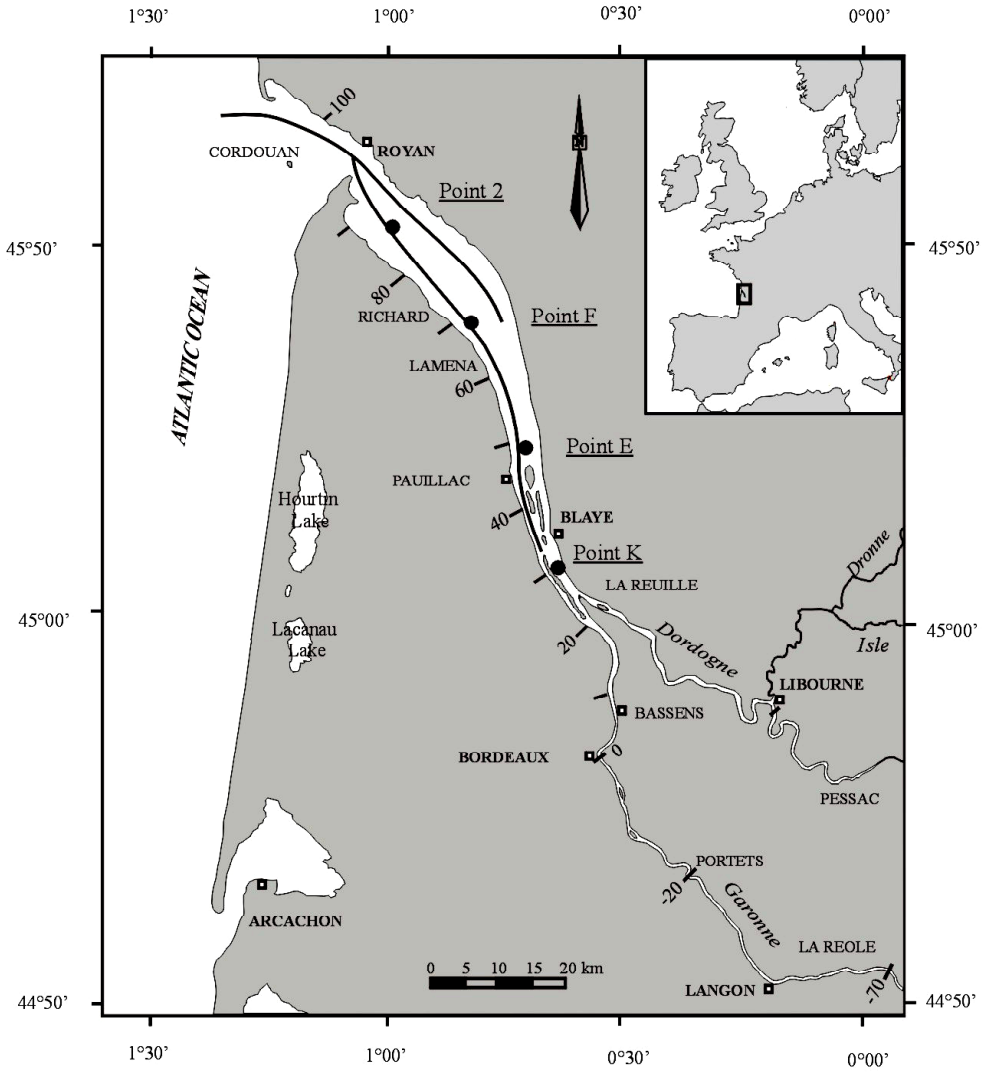


*Figure 1: Map of the Gironde estuary (South-West of France). The black thick lines represent the main channels. The four black circles locate the fixed stations where most of the field measurements were carried out. The estuary is delimited by kilometre points (KP); KP 0 is Bordeaux (Garonne River) and KP 90 is the mouth.*

The SPOT-HRV and Landsat-ETM+ sensors were selected for this study, due to their spatial resolution (20 m and 30 m, respectively) that is spatially consistent with the dimensions of estuaries. The SPOT-HRV sensor has two wavebands in the visible, XS1 (500-590 nm) and XS2 (610-680 nm), and one waveband in the NIR, XS3 (790-890 nm) (22). The Landsat-ETM+ sensor has three bands in the visible, L1 (450-515 nm), L2 (525-605 nm) and L3 (630-690 nm), and two bands in the NIR, L4 (750-900 nm) and L5 (1550-1750 nm) (23). Seven satellite images of the Gironde estuary were considered in this study: six SPOT images recorded in 1996 and 2001; one Landsat image recorded in 2000 (see Table 1 for details). These images were selected at different periods of the year, in order to illustrate the seasonal movements of the MTZ.

*Table 1: Details of the satellite images of the Gironde estuary. $\theta_v$ is the viewing zenith angle.*

| **Date** | Time (GMT) | Satellite | Sensor | $\theta_v$ (°) |
|---|---|---|---|---|
| 14/07/1996 | 11h23'40 | SPOT-3 | HRV-1 | + 23.7 |
| 08/03/2000 | 10h40'22 | Landsat-7 | ETM+ | + 00.0 |
| 20/05/2001 | 11h10'23 | SPOT-2 | HRV-1 | + 01.2 |
| 31/05/2001 | 10h58'50 | SPOT-2 | HRV-2 | - 15.4 |
| 31/05/2001 | 11h30'51 | SPOT-1 | HRV-2 | + 27.5 |
| 02/07/2001 | 11h15'49 | SPOT-1 | HRV-1 | + 05.9 |
| 17/08/2001 | 11h31'53 | SPOT-1 | HRV-1 | + 30.0 |

Two difficulties were encountered when applying the atmospheric correction scheme. The first one was to locate black targets on the satellite images. These targets were located where the $R^*$ signal was minimum in the NIR. Depending on the satellite images, these targets were lake waters or continental shelf waters beyond the influence of the turbid plume (Table 2). On the SPOT image recorded on 17/08/2001 and covering the central and upstream parts of the estuary, these selected black targets (open ocean or lake waters) didn't appear. The 6S aerosol model was consequently determined according to the meteorological data (wind speed and direction, horizontal visibility) available at different stations around the estuary. The second difficulty was the number of SPOT spectral bands in the NIR. Only one NIR band (XS3) was available for the sensor onboard the SPOT 1, 2 and 3 satellites. In order to calculate the Ångström coefficient (eq. 9), it was consequently assumed that the water-leaving radiance in the red band (XS2) was also zero. Such an assumption may have lead to a slight overestimation of the aerosol contribution. Concerning the Landsat data, the L4 and L5 NIR bands were selected to calculate the Ångström coefficient.

*Table 2: Satellite atmospheric correction parameters, i.e. the selected 6S atmospheric and aerosol models (DL = dust-like; WS = water soluble; O = oceanic and S = soot), the black target on the image, and the corresponding vertical visibility.*

| **Date** | 6S atm. model | Black target | 6s 6S aerosol model | Vis. /km |
|---|---|---|---|---|
| 14/07/1996 | Midlatitude Summer | Hourtin lake | 39% DL, 15% WS, 40% O, 1% S | 13 |
| 08/03/2000 | Midlatitude Winter | Lacanau Lake | 95% O, WS 5% | 15 |
| 20/05/2001 | Midlatitude Summer | Hourtin lake | 50% DL, 50% O | 20 |
| 31/05/2001 (a) | Midlatitude Summer | Continental shelf waters | 39% DL, 15% WS, 40% O, 1% S | 9 |
| 31/05/2001 (b) | Midlatitude Summer | Lacanau Lake | 4% DL, 6% WS, 90% O | 12 |
| 02/07/2001 | Midlatitude Summer | Continental shelf waters | 70% DL, 29% WS, 1% S | 10 |
| 17/08/2001 | Midlatitude Summer | - | 70% DL, 29% WS, 1% S | 15 |

## RESULTS

### Calibration relationships

In turbid sediment-dominated waters, improved calibration relationships can be established between $R_{rs}$ ratios and *SPM*. Such results were first obtained from theoretical calculations (6) or using a bio-optical model (7). They were confirmed by numerous field measurements carried out in two different estuaries (7-9). In turbid sediment-dominated waters, $R_{rs}$ ratios between two NIR bands or between a NIR and a visible band are highly correlated to *SPM*. Such $R_{rs}$ ratios are relatively insensitive to the characteristics of the suspended sediments (6-9), and relatively insensitive to changing illumination conditions (notably the cloud cover) at the moment of field optical measurements (9).

As a consequence, invariant relationships have been established between $R_{rs}$ ratios and *SPM* in the Gironde estuary, from numerous field measurements carried out during a six years study (9). Similar relationships have been established in the Loire estuary from field measurements carried out during a three months study (9). In the Gironde estuary, the relationships were established from 18 data points in 1996, 27 in 1997, 32 in 1999, 39 in 2000 and 16 in 2001. Different conditions of tide, river flow and cloud cover were encountered during the field measurements essentially carried out in four fixed stations (Figure 1) representative of the different parts of the estuary. As a result, invariant exponential calibration curves were established between $R_{rs}$ ratios in SPOT bands (XS3 / XS1, Figure 2A) or Landsat bands ((L4 / L2, Figure 2B) and *SPM* in the range 15 – 2000 mg $l^{-1}$.

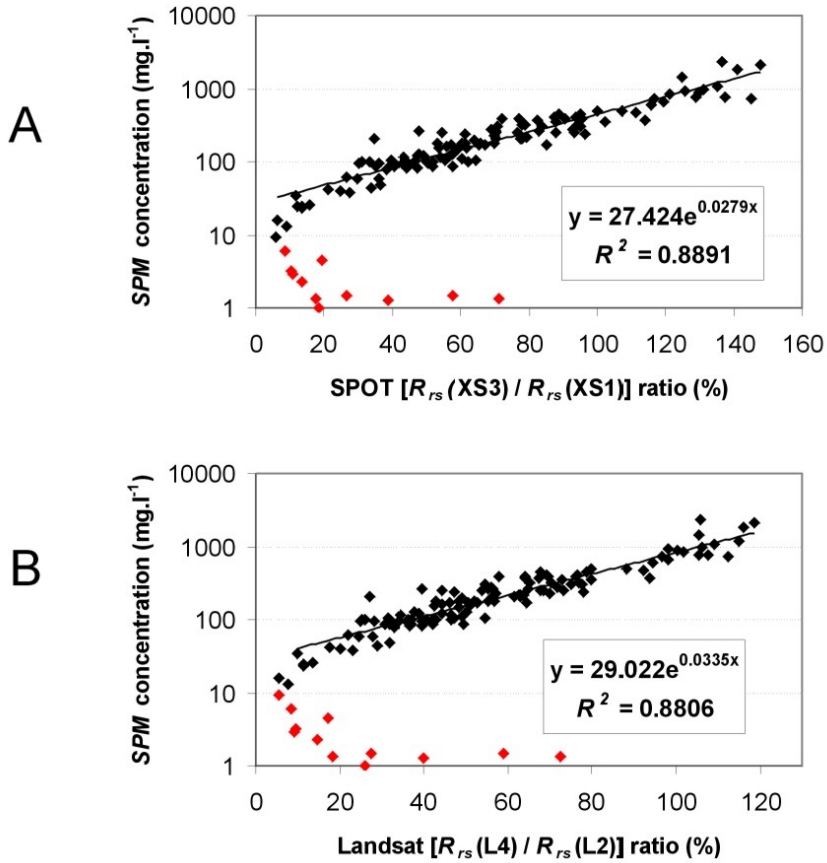


*Figure 2: Calibration curves established in the Gironde estuary from field measurements carried out between 1996 and 2001 and used to calculate $R_{rs}$ in: A) SPOT-HRV bands. B) Landsat-ETM+ bands. Red points show the data collected in the turbid plume, with corresponding SPM lower than 10 mg $l^{-1}$.*

The $R_{rs}$ ratios increase with increasing *SPM*. These calibration curves are valid at least for the 1996 – 2001 period. They can be used to compute *SPM* from satellite data recorded during this period even if no field measurements were carried out at the moment of the satellite overpass, which was the initial objective of the study. However, the established calibration curves also present a limit of applicability. In fact, measurements carried out in the turbid plume of the Gironde (red points on Figure 2), corresponding to *SPM* values lower than 10 mg $l^{-1}$, are not included in the relationships. For such low turbidity, the $R_{rs}$ signal in the NIR is close to zero (few sensitive to *SPM*), and is low in the visible. The considered ratio is thus a ratio between two values close to zero, which may explain the observed divergence. Changing surface reflection effects induced by the rough sea surface out of the estuary is another factor to be considered. These reflection effects, imperfectly corrected in eq. (11) ($\rho$ values were selected according to the cloud cover only), may have resulted in significant errors when determining $L_W$. In-water optical measurements would be more appropriate and may permit to conclude. At this stage, the established calibration curves are only valid for the Gironde estuarine waters where *SPM* is higher than 10 mg $l^{-1}$.

In the Loire estuary, relationships where established from 66 data recorded in 2002 (39 in February, 11 in March and 16 in April) during flood events. Different conditions of tide and cloud cover were encountered during the field measurements carried out in the central and downstream parts of the estuary (9). As a result, an invariant exponential calibration curve was established between the $R_{rs}$ ratio in SPOT bands (XS3 / XS1, Figure 3A) and *SPM* in the range 40 – 2600 mg $l^{-1}$. Its validity, at least for the February to March 2002 period, can be used to calibrate satellite data from the estuary. The calibration curve in SPOT bands is different from the one established in the Gironde, resulting from different characteristics of the suspended sediments in the two estuaries (9). From our hyperspectral $R_{rs}$ measurements, equivalent calibration relationships can be adapted to any satellite sensor, such as SeaWiFS (Figure 3B).

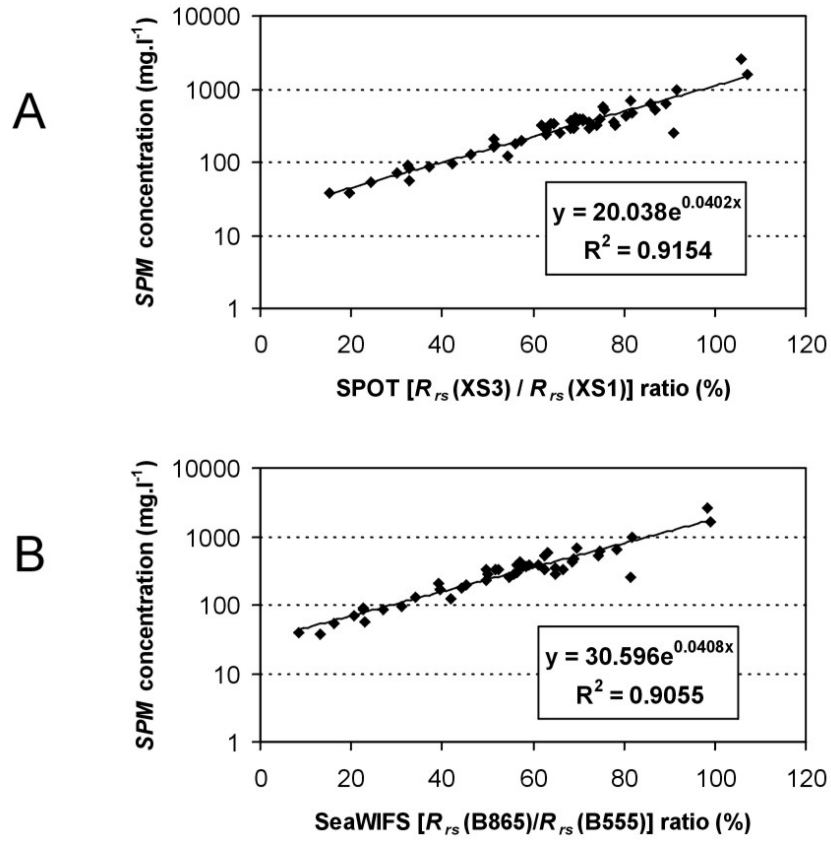


*Figure 3: Calibration curves established in the Loire estuary from field measurements carried out in February, March and April 2002 and used to calculate $R_{rs}$ in: A) SPOT-HRV bands, B) SeaWiFS bands.*

**Atmospheric corrections**

The satellite atmospheric correction has been processed assuming that the atmosphere was homogeneous over the whole estuary. The established relationships between $R^*$ and $R_w$ are practically linear (7). Such an assumption does not take into account the "pixel by pixel" correction scheme universally adopted for ocean colour sensors, which requires at least two wavebands in the NIR and a good knowledge of the inherent optical properties of the water body (e.g. 6). However, it is interesting to note, according to these results, that the water reflectance signal was predominant compared to the atmospheric contribution (Table 3). In clear oceanic waters, the water-leaving signal generally represents about 10% of the signal at the top of the atmosphere (24). Using the established calibration curves, the logarithm of the *SPM* concentration in the range (10 – 2000 mg $l^{-1}$), and so of the water turbidity, is proportional to the reflectance ratio $R_{rs}(NIR)/R_{rs}(VIS)$. It is thus possible to locate on each satellite image the pixels corresponding to the minimum, mean and maximum turbidity. On these pixels, the ratio $R_w/R^*$ represents the percentage of the signal measured onboard the satellite, at the top of the atmosphere, due to the water-leaving signal, i.e. the respective contributions of water and atmosphere within the satellite measurements. For low turbidity, it appears that the water-leaving signal represents more than 60% of the total signal (Table 3). The atmospheric contribution is always higher in the NIR than in the visible, and minimum in the red part of the spectrum. Concerning the mean turbidity pixels, the atmospheric contribution strongly decreases and is typically lower than 10% of the total signal. For the maximum turbidity, the atmosphere contribution becomes practically insignificant (lower than 3%), especially in the red and NIR. These obtained results are due to the high concentrations of suspended solids in water, that involve a high scattering and notably backscattering of the incident irradiance. This is contrary to clear ocean waters where absorption by pure seawater is usually high compared to the scattering properties of phytoplankton. As a practical consequence, and according to the obtained results, the uncertainty of the atmospheric correction only slightly affects the uncertainty of the retrieved *SPM*. The *SPM* retrieval uncertainty thus essentially depends on the calibration relationships based on $R_{rs}$ ratios.

*Table 3: Examples of the atmospheric correction results, for three SPOT images of the Gironde estuary. Relative importance of the water reflectance compared to the signal measured onboard the satellite, expressed as the $R_w/R^*$ ratio (in %), when considering the minimum, mean and maximum retrieved SPM.*

| Satellite image date | Spectral band | | $R_w$ / $R^*$ (%) | |
|---|---|---|---|---|
| | | Minimum turbidity | Mean turbidity | Maximum turbidity |
| | XS1 | 79 | 93 | 87 |
| 20/05/2001 | XS2 | 83 | 92 | 97 |
| | XS3 | 60 | 93 | 99 |
| | XS1 | 76 | 96 | 94 |
| 02/07/2001 | XS2 | 83 | 97 | 98 |
| | XS3 | 64 | 98 | 99 |
| | XS1 | 89 | 92 | 95 |
| 17/08/2001 | XS2 | 93 | 97 | 98 |
| | XS3 | 72 | 98 | 99 |

**Application: seasonal movements of the MTZ in the Gironde estuary**

After applying the atmospheric correction, the calibration relationships established in the Gironde were applied to the satellite data. Horizontal distributions of turbidity within the surface waters of

the estuary were established for each satellite image, locating the MTZ and observing its seasonal movements.

The first image (SPOT-HRV, 14/07/1996, 11h23) describes the situation during a low river flow period, for mean tides. It was recorded during the start of the flood in the downstream part of the estuary, corresponding to the low water slack tide in the central part and the ending ebb in the upstream part. Decreasing *SPM* was observed from the upstream part to the mouth (Figure 4A). Two MTZ were located: one in the central part of the estuary, around the islands and a second upstream at the confluence zone of the rivers. High *SPM* concentrations were observed along the main navigation channel, along the left shores, where suspended sediments were transported downstream during the ebb tide.

The second image (Landsat-ETM+, 08/03/2000, 10h40) is representative of very different conditions: spring tides and high river flow (peak flood). It was taken around mid ebb in the central part of the estuary. High *SPM* concentrations were observed in the whole estuary (Figure 4B). The lowest *SPM* concentrations were located in the rivers and in the upstream part. Resulting from successive floods, the MTZ moved into the central and downstream parts of the estuary, and was partly expelled towards the ocean during the ebb.

The third image (SPOT-HRV, 20/05/2001, 11h10) was recorded during mean tides, the last day of a six-month long high river flow period. As a consequence, the *SPM* concentrations were low in the whole estuary (Figure 4C). A “residual” MTZ, after being partly expelled in the ocean, was located in the central part of the estuary. High *SPM* were also observed in front of the point kilometre (PK) 60, probably resulting from resuspension over mud banks.

The river flow rapidly decreased after 20/05/2001. Ten days later, two satellite images (SPOT-HRV, 31/05/2001, 10h58 and 11h30, respectively) show the influence on the location of the MTZ. As a result of the decreasing river flow, it moved rapidly upstream (estimated mean velocity of 1.4 km per day), reaching the confluence zone of the Garonne and Dordogne rivers (Figure 5A). High *SPM* concentrations were still observed in front of the PK 60.

The next image (SPOT-HRV, 02/07/2001, 11h16) only concerned the central and downstream parts of the estuary. It was taken for mean tides, at the beginning of the low river flow period. According to the established *SPM* map (Figure 5B), the MTZ was still located in the central and upstream parts. Downstream, turbid features were observed over most of the mud and sandbanks, resulting from resuspension phenomena.

The last image (SPOT-HRV, 17/08/2001, 11h32) concerned the central and upstream parts of the estuary. It was recorded for mean tides, after a three-month long low river flow period. As a consequence, the main MTZ moved into the rivers (Figure 5C), but a secondary one was also observed in the central part of the estuary, where sediments were trapped in the island zone. Resuspension phenomena were still observed over mud banks in front of the KP 60, which finally resulted in a global 70 km-long MTZ.

To summarise, the following observations were made on the different images.

- the range of the retrieved *SPM* was always totally realistic according to the previous field turbidity measurements carried out in the estuary (e.g. 25,26,27). These results indirectly validate the applied algorithm. However, a rigorous validation based on simultaneous *in situ* optical measurements and satellite data acquisition is needed;
- the seasonal movements of the MTZ observed or deduced from the analysed satellite images were also in agreement with previous observations (e.g. 23-25) and with recent observations made from turbidity profiles regularly measured at different fixed stations in 2001 (28).

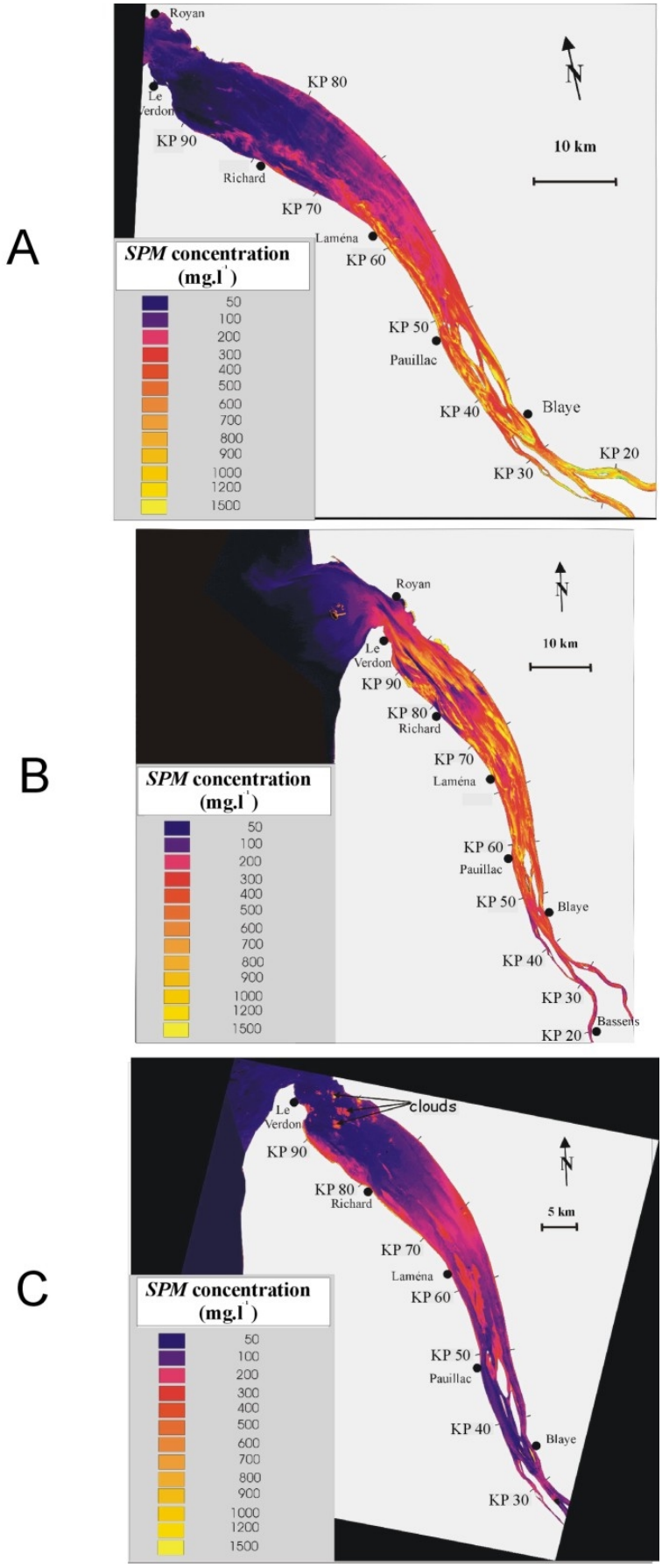


*Figure 4: SPM maps established from satellite data of the Gironde estuary. A) SPOT-HRV 14/07/1996, 11h23. B) Landsat-ETM+ 08/03/2000, 10h40. C) SPOT-HRV 20/05/2001, 11h10.*

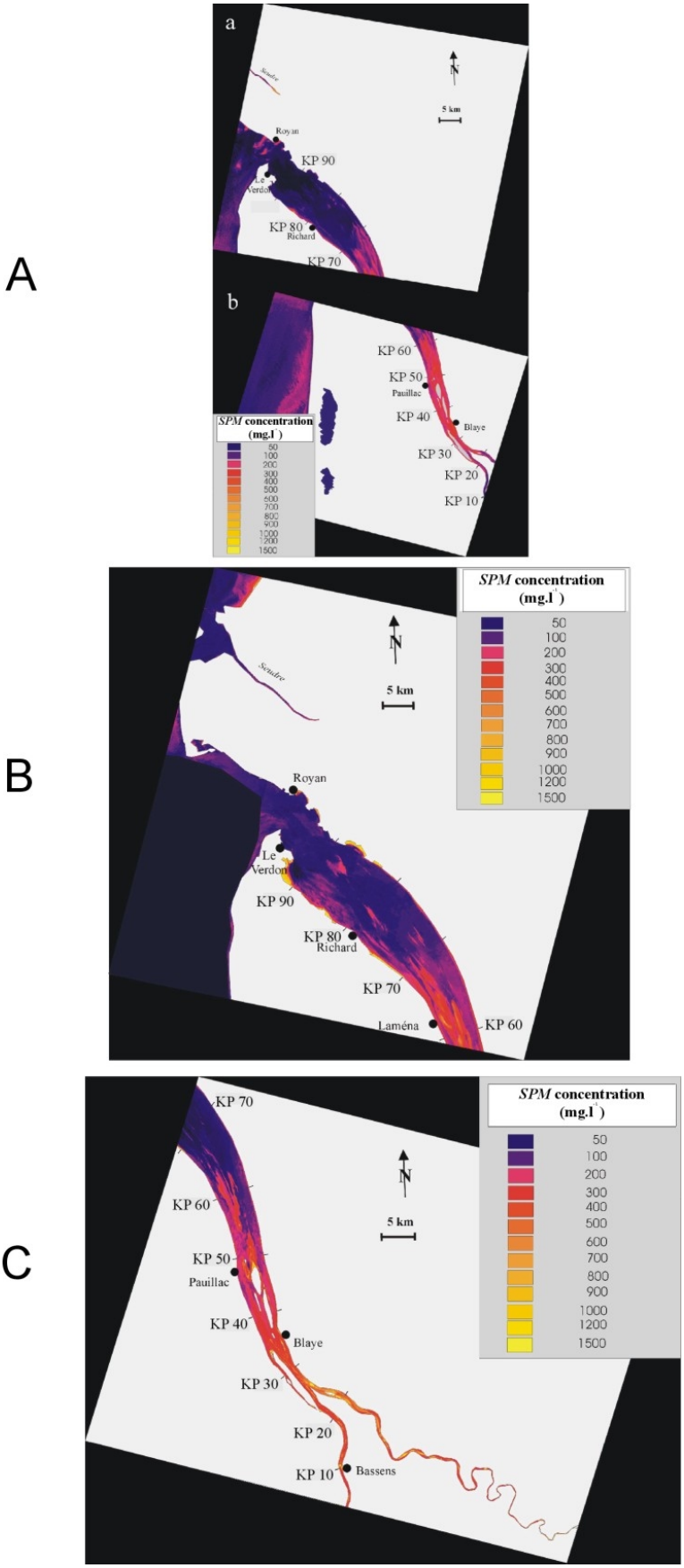


*Figure 5: SPM maps established from satellite data of the Gironde estuary. A) SPOT-HRV 31/05/2001, 10h58 (a) and 11h30 (b). B) SPOT-HRV 02/07/2001, 11h16. C) SPOT-HRV 17/08/2001, 11h32.*

## CONCLUSIONS

A simple and operational method was presented to quantify the suspended sediment concentrations in turbid estuarine waters using satellite imagery. Results were obtained from applying the method to a set of images from the Gironde estuary

The method is based on calibration relationships between $R_{rs}$ ratios (NIR / VIS) and suspended sediment concentrations. Such relationships are invariant and valid for a long-term, because $R_{rs}$ ratios are relatively insensitive to the variations of the sediment characteristics and relatively insensitive to illumination conditions. They provide satellite estimates without field measurements during the satellite overpass. They have been established for two different estuarine environments (the Gironde and the Loire, in France) and may be extended to most of the turbid sediment-dominated coastal waters. Current research aims at reproducing the results using a theoretical reflectance model, in order to develop improved algorithms for satellite and airborne sensors. The model will determine the calibration relationship from the sediment characteristics in a studied area and according to the sensitivity of the selected optical sensor (e.g. MERIS, MODIS, CHRIS-PROBA).

Before applying the established relationships, satellite data were corrected for atmospheric effects, assuming that the atmosphere was homogeneous over the whole selected image. This simple correction scheme will be improved, using recent “pixel by pixel” correction schemes (e.g. 6). However, an important result was revealed: the reduced influence of the atmosphere on satellite data over highly scattering turbid estuarine waters. As a consequence, the *SPM* retrieval uncertainty essentially depends on the calibration relationships between the $R_{rs}$ signal and *SPM*.

The method was applied to satellite data from the Gironde estuary. Concluding results were obtained in terms of retrieved sediment concentrations and turbidity maps. Because of the limited influence of the atmosphere on satellite data from such highly turbid waters (Table 3), the accuracy of the estimated sediment concentrations essentially depends on the established calibration relationships (Fig. 2 and 3). This accuracy is already satisfactory but may be increased by improving the field measurement techniques (e.g. measuring in-water the upwelling radiance signal to remove the surface reflection effects). The high spatial resolution of the SPOT and Landsat sensors can be used to locate the seasonal movements of the MTZ, and gives observation of detailed turbidity features resulting from resuspension phenomena. Such information can be used to calibrate and validate numerical transport models (1, 2). The applied method still needs to be validated with match-ups (simultaneous in situ and remote sensing measurements). The method will soon be applied to airborne imagery (e.g. CASI), which will facilitate its validation.

## ACKNOWLEDGEMENTS

This study was financed by the Conseil General d’Aquitaine (France), and partly supported through a European Community Marie Curie fellowship (NCR 70037, Fifth Framework Programme).

## REFERENCES

1 Siegel H, M Gerth & A Mutzke, 1999. Dynamics of the Oder river plume in the Southern Baltic Sea: satellite data and numerical modelling. Continental Shelf Research, 19: 1143-1159

2 Douillet P, S Ouillon & E Cordier, 2001. A numerical model for fine suspended sediment transport in the south-west lagoon of New-Caledonia. Corals Reefs, 20: 361-372

3 Bowers D G, S Boudjelas & G E L Harker, 1998. The distribution of fine sediments in the surface waters of the Irish Sea and its relation to tidal stirring. International Journal of Remote Sensing, 19: 2789-2805

4 Robinson M C, K P Morris & K R Dyer, 1998. Deriving fluxes of suspended particulate matter in the Humber estuary, UK, using airborne remote sensing. Marine Pollution Bulletin, 37: 155–163

5 Froidefond J M, P Castaing & R Prud'homme, 1999. Monitoring suspended particulate matter fluxes and patterns with the AVHRR/NOAA-11 satellite: application to the Bay of Biscay. Deep Sea Research II, 46: 2029–2055

6 Moore G F, J Aiken & S J Lavender, 1999. The atmospheric correction of water colour and the quantitative retrieval of suspended particulate matter in Case II waters: Application to MERIS. International Journal of Remote Sensing, 20: 1713-1733

7 Doxaran D, J M Froidefond, S J Lavender & P Castaing, 2002a. Spectral signature of highly turbid waters. Application with SPOT data to quantify suspended particulate matter concentrations. Remote Sensing of Environment, 81: 149-161

8 Doxaran D, J M Froidefond & P Castaing, 2002b. A reflectance band ratio used to estimate suspended matter concentrations in sediment-dominated coastal waters. International Journal of Remote Sensing, 23: 5079-5085

9 Doxaran D, J M Froidefond & P Castaing, 2003. Remote sensing reflectance of turbid sediment-dominated waters. Reduction of sediment type variations and changing illumination conditions effects using reflectance ratios. Applied Optics, 42: 2623-2634

10 Vermote E F, D Tanre, J L Deuze, M Herman & J J Morcrette, 1997. Second Simulation of the Satellite Signal in the Solar Spectrum: An Overview. IEEE Transactions in Geosciences and Remote Sensing, 35: 675-686

11 Antoine D & A Morel, 1998. Relative importance of multiple scattering by air molecules and aerosols in forming the atmospheric path radiance in the visible and near-infrared parts of the spectrum. Applied Optics, 37: 2245-2259

12 Mobley C D, 1999. Estimation of the remote-sensing reflectance from above-surface measurements. Applied Optics, 38: 7442-7455

13 Morel A & L Prieur, 1977. Analysis of variations in ocean color. Limnology and Oceanography, 22: 709-722

14 Gordon H R, O B Brown & M M Jacobs, 1975. Computed relation between the inherent and apparent optical properties of a flat homogeneous ocean. Applied Optics, 14: 417-427

15 Morel A & B Gentili, 1993. Diffuse reflectance of oceanic waters. II. Bidirectional aspects. Applied Optics, 32: 6864-6879

16 Morel A & B Gentili, 1996. Diffuse reflectance of oceanic waters. III. Implication of bidirectionality for the remote-sensing problem. Applied Optics, 35: 4850-4861

17 Loisel H & A Morel, 2001. Non-isotropy of the upward radiance field in typical coastal (Case 2) waters. International Journal of Remote Sensing, 22: 275-295

18 Forget P, S Ouillon, F Lahet & P Broche, 1999. Inversion of reflectance spectra of non-chlorophyllous turbid coastal waters. Remote Sensing of Environment, 68 : 264-272

19 Chavez P S Jr., 1988. An improved dark-object substraction technique for atmospheric scattering correction of multispectral data. Remote Sensing of Environment, 24: 459-479

20 Angstrom A, 1964. The parameters of atmospheric turbidity. Tellus, 16: 64-75

21 Fougnie B, R Frouin, P Lecomte & P Y Deschamps, 1999. Reduction of skylight reflection effects in the above-water measurements of diffuse marine reflectance. Applied Optics, 38: 3844-3856

22 http://www.spotimage.fr/accueil/system/introsat/select/welcome.htm

23 http://landsat.gsfc.nasa.gov/guides/LANDSAT-7_dataset

24 Mobley C D, 1994. Light and water. (Academic Press) 592 pp.

25 Allen G P, G Sauzay, P Castaing & J M Jouanneau, 1977. Sediment transport processes in the Gironde estuary. In Estuarine processes, edited by M Wilet (Academic Press, New York), p. 63-81

26 Castaing P, 1981. Le transfert à l'océan des suspensions estuariennes. Cas de la Gironde. Thèse d'Etat, Université Bordeaux I, n° 701, 530 p.

27 Sottolichio A, P Le Hir & P Castaing, 2001. Modelling mechanisms for the turbidity maximum stability in the Gironde estuary, France. In: Coastal and estuarine fine sediment transport processes, edited by W H McAnally & A J Mehta (Elsevier, Amsterdam), p. 373-385

28 Doxaran D, 2002. Teledetection & modelisation des flux sedimentaires dans l'estuaire de la Gironde. These de 3eme Cycle, Universite Bordeaux 1, n° 2612, 284 p.